Journal of Structural Geology, Vol. 14, No. 3, pp. 301 to 313, 1992
Printed in Great Britain

0191-8141/92 $05.00+0.00

Phase boundary mobility in naturally deformed, high-grade quartzofeldspathic rocks: evidence for diffusional creep

ROBERT J. W. GOWER and CAROL SIMPSON

Department of Earth and Planetary Sciences, The Johns Hopkins University, Baltimore, MD 21218, U.S.A.

(*Received* 20 *November* 1990; *accepted in revised form* 28 *July* 1991)

Abstract—Grain shape fabrics and optical microstructures of some quartzofeldspathic rocks deformed under upper amphibolite facies conditions in the southwestern Grenville Province, Ontario, Canada, suggest that quartz and feldspar have accommodated intracrystalline plastic strains by both diffusional and dislocation creep. In these rocks, quartz and feldspar form polycrystalline domains separated by gently curved and locally cuspate phase boundaries whose morphology is similar in certain respects to the phase boundary morphology of rocks annealed experimentally under hydrostatic stress conditions. In the naturally deformed rocks, however, phase boundary cusps consistently point along the foliation and parallel to the mineral fibre lineation (i.e. in directions of inferred finite extension) which implies that phase boundary motion and cusp formation occurred during deformation.

Optical microstructures in feldspar and crystallographic preferred orientations in quartz are consistent with the accommodation of some intracrystalline plastic strains by dislocation creep. However, the morphology of quartz–feldspar phase boundaries cannot be explained by either dislocation creep or static annealing alone. We propose that phase boundary motion resulted from a diffusion-assisted process involving dissolution at foliation-parallel quartz–feldspar phase boundaries, mass transfer over length scales of the order of feldspar domain size (~200 μm or greater) and precipitation at quartz–feldspar phase boundary cusps.

This study extends the range of natural deformation conditions under which diffusional creep has been identified in quartzofeldspathic rocks. It also has important implications for the natural rheological behavior of the mid- and lower-continental crust.

INTRODUCTION

ONE of the aims of microstructural analysis is to identify the grain scale processes that control the formation and motion of phase and grain boundaries through rocks during and after deformation. Textural evidence for syndeformational grain boundary motion, or dynamic recrystallization, has been recognized in experimentally deformed mineral analogues (Urai 1983, Drury *et al.* 1985, Burg *et al.* 1986) and in many naturally and experimentally deformed minerals (e.g. calcite—Schmid *et al.* 1987; feldspar—Tullis & Yund 1985, White & Mawer 1988; halite—Guillope & Poirier 1979; quartz—White 1976). In these examples, recrystallization is a conservative process in which grain boundaries form and migrate through monomineralic areas of a material with only slight changes in chemical composition and crystal structure (Urai *et al.* 1986). In contrast, geochemical studies (e.g. Beach 1976, Dipple *et al.* 1990) indicate that chemically-induced mass transport is common during deformation in many natural settings. This process is expected to produce grain shape fabrics which result not only from isochemical dynamic recrystallization but also from the effects of grain scale reaction and diffusion.

Previous microstructural studies of naturally deformed quartz, alkali and plagioclase feldspars at temperatures greater than 550°C have placed considerable emphasis on the importance of dislocation creep as a strain-accommodating mechanism. For example, Lister & Dornsiepen (1982) and Blumenfeld *et al.* (1986) have reported quartz *c*-axis preferred orientations in granulite and upper amphibolite grade tectonites consistent with activation of the prism ⟨*c*⟩ glide systems in quartz. Crystallographic preferred orientations consistent with dislocation motion on the (010)[001] and (010)[100] glide systems in plagioclase have been reported by Ji & Mainprice (1988). Microstructures consistent with dislocation creep are also widely reported from optical and transmission electron microscopic (TEM) observations of naturally deformed plagioclase (Gandais & Willaime 1983, Olsen & Kohlstedt 1984, Montardi & Mainprice 1987) and alkali feldspar (White & Mawer 1986, 1988).

Microstructures consistent with diffusional creep in high-grade quartzofeldspathic rocks are less widely reported. Evidence for diffusional creep in experimentally deformed quartzofeldspathic rocks at elevated temperatures is largely restricted to grain sizes of 10 μm or less (see review by Tullis 1990). The process is also enhanced by the presence of a granitic partial melt (Dell'Angelo & Tullis 1988). Microstructural criteria for diffusional creep under these conditions include grain indentation, evidence for fine-scale dissolution and low dislocation densities (Dell'Angelo & Tullis 1988). Grain indentation and grain overgrowths (Mosher 1981) and truncation of compositional zoning (Walton *et al.* 1964) have been used as criteria for diffusional mass transfer in naturally deformed rocks. In addition, diffusion-accommodated grain boundary sliding has been shown to occur in some high temperature quartzofeldspathic mylonites (Behrmann & Mainprice 1987) in which extreme plastic strains are accommodated by a steady-state microstructure of very fine, internally strain-free grains.

We report the microstructures of quartzofeldspathic rocks deformed under upper amphibolite facies conditions in the southwestern part of the Grenville Province (Wynne-Edwards 1972) near Parry Sound, Canada, where White & Mawer (1986, 1988) reported the preservation of extreme intracrystalline plastic strains in perthitic alkali feldspars. Emphasis is placed here on the geometric and morphological characteristics of cuspate quartz–feldspar phase boundaries in these rocks and attention is drawn to the similarities between these microstructures and the cuspate grain-shape fabrics of statically annealed rocks (e.g. Kretz 1966, Spry 1969, Vernon 1970). The preserved microstructures are inconsistent with phase boundary motion resulting from either static annealing or dislocation creep alone; we propose an additional recrystallization mechanism by which this motion occurred.

GEOLOGICAL SETTING

Samples were collected from an area south-southwest of Parry Sound, Ontario, Canada (80°01′W to 80°12′W and 45°07′N to 45°17′N), within the Central Gneiss Belt of the Grenville Province (Wynne-Edwards 1972) (Fig. 1). The area lies within the Parry Sound Domain of Davidson (1984). There are three groups of rocks in the area (Culshaw *et al.* 1988): (a) felsic and mafic para- and orthogneisses that include some supracrustal gneisses; (2) several meters to 7 km thick bodies of anorthosite and gabbroic anorthosite within group 1 gneisses; and (3) quartzofeldspathic, syn- and post-tectonic pegmatites with grain sizes of 5 mm to 30 cm.

Deformation occurred during the Grenville orogeny at about 1.1 Ga (van Breeman *et al.* 1986), when early recumbent folds that close to the northeast were refolded by late upright folds with NW-striking axial surfaces (Schwerdtner 1987). Late fold axes are consistently parallel to a strong quartz–feldspar fibre lineation. Deformation was under granulite to upper amphibolite facies conditions with peak metamorphic temperatures of 750 ± 50°C and pressures of 10 ± 1 kb (Anovitz & Essene 1990).

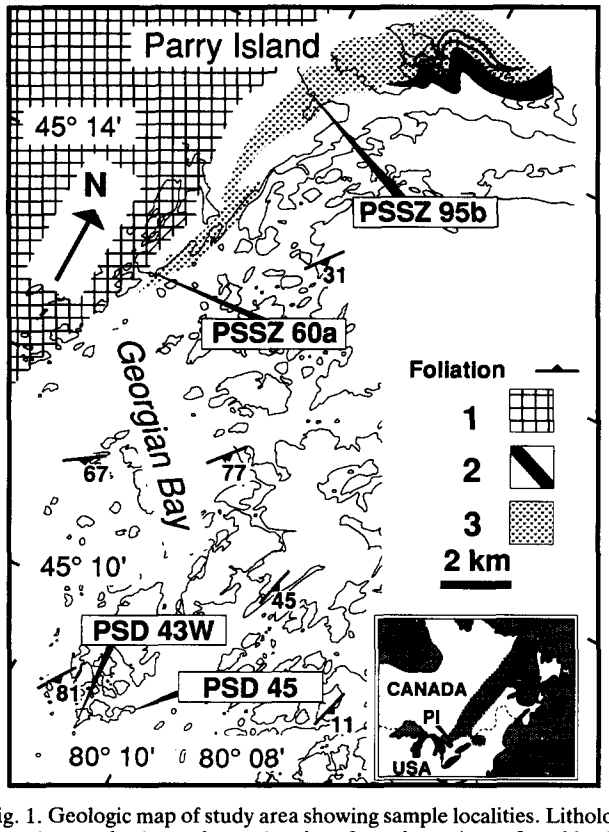

Fig. 1. Geologic map of study area showing sample localities. Lithologies: 1, anorthosite and associated mafic orthogneisses; 2, gabbroic anorthosite; 3, meta-sedimentary paragneisses including migmatic semipelite and quartz-rich gneiss. Unstippled: undifferentiated quartzofeldspathic and mafic gneisses. Inset: Grenville Province. PI Parry Island.

GEOTHERMOMETRY

Closure temperatures for Fe–Mg exchange between garnet and biotite were estimated in PSD 45, a quartzofeldspathic gneiss, and in PSSZ 95b, a quartz-rich gneiss. Petrographic details for both samples are given in the Appendix. A pressure of 10 kb was assumed and is consistent with the results of a previous thermobarometric study in the area by Anovitz & Essene (1990). Representative garnet-rim and biotite compositions are given in Table 1. In PSD 45, garnet is present as foliation-parallel trails of anhedral, 200 μm–2 mm long grains; biotite compositions were determined on foliation-parallel, 150–400 μm long grains adjacent to

Table 1. Representative electron microprobe analyses of garnet-rim and biotite compositions in PSD 45 and PSSZ 95b. See text for microstructural details

	PSD 45		PSSZ 95b	
	garnet	biotite	garnet	biotite
Na_2O	0.05	0.06	0.07	0.06
MgO	5.25	12.99	2.64	8.93
Al_2O_3	21.66	15.31	21.37	16.24
SiO_2	37.55	36.58	37.88	36.27
K_2O	0	9.65	0	9.53
CaO	2.00	0.09	8.22	0.08
TiO_2	0.05	0.09	0.08	4.18
Cr_2O_3	0.10	0	0	0.05
MnO	1.52	0	3.91	0.16
FeO_T^*	32.57	17.08	26.96	21.21
Total	100.76	96.48	101.13	96.71
	Cations for 24 oxygens			
Na	0.017	0.019	0.210	0.020
Mg	1.233	3.155	0.620	2.204
Al	4.028	2.941	3.969	3.167
Si	5.924	5.960	5.968	6.004
K	0	2.006	0	2.013
Ca	0.337	0.016	1.387	0.014
Ti	0.005	0.579	0.009	0.520
Cr	0.012	0	0	0.006
Mn	0.204	0	0.522	0.022
Fe	4.298	2.327	3.552	2.936
X_{Fe}	0.708	0.424	0.584	0.571
X_{Mg}	0.203	0.576	0.102	0.429

*All Fe reported as Fe^{2+}.

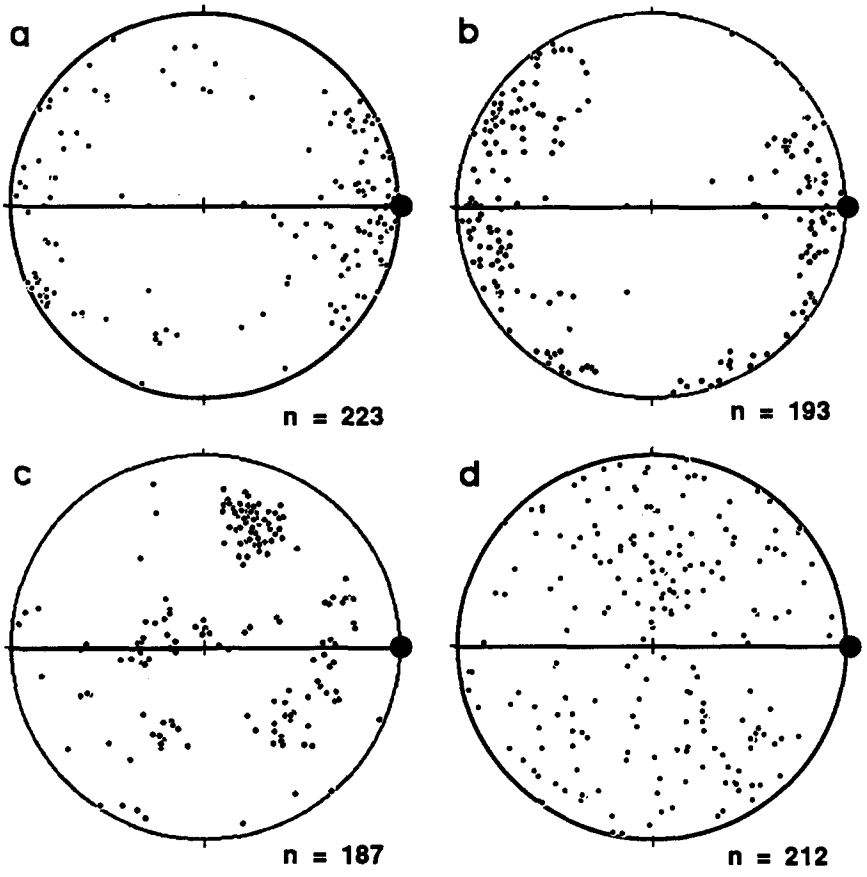

Fig. 2. Lower-hemisphere stereographic projections of quartz c-axes. (a) PSD 43W, (b) PSSZ 95b, (c) PSSZ 60a, (d) PSD 45.

microprobed garnet grains. Microprobe traverses of garnet grains found no evidence of compositional zoning. In PSSZ 95b, ~100 μm long biotite grains and euhedral, ~300 μm long garnet grains are present in a garnet–plagioclase–biotite–quartz layer in which biotite has a strong grain shape preferred orientation parallel to compositional layering. Garnet-rim and biotite compositions were obtained from adjacent grains in this sample.

Following the garnet–biotite geothermometry methods of Ferry & Spear (1978) and Hodges & Spear (1982), respectively, closure temperatures were estimated at 660 ± 50°C and 680 ± 50°C in PSD 45, and 700 ± 50°C and 740 ± 50°C in PSSZ 95b. These temperatures are probably a minimum estimate of deformation temperatures in the samples.

MICROSTRUCTURES

In hand sample, the mineral fibre lineation is defined by elongate quartz and feldspar grains. Foliations in all samples are defined by polycrystalline quartz ribbons, a grain-shape preferred orientation of biotite, and parallel trails of 40–500 μm feldspar. In sample PSD 45, the foliation is offset by shear bands that are inclined at 40–45° to the foliation. Orthogonal thin sections were cut parallel and perpendicular to the mineral fibre lineation and parallel and perpendicular to the foliation. Petrographic details of each sample are given in the Appendix.

Quartz

With the exception of an occasional subgrain boundry, quartz is free of optically-detectable intracrystalline plastic strain. To a first approximation, the grain size of quartz observed in thin section is inversely proportional to the modal volume of feldspar and biotite present. As a consequence, grain sizes are generally larger in the quartz-rich gneisses (PSSZ 60a and PSSZ 95b) than in the quartz-poor ones. In all samples, however, grain sizes range from 200 μm to 2 mm. In the absence of other minerals, quartz grain shapes are irregular and amœboid. Where polycrystalline quartz ribbons are developed they contain rectangular or irregularly-shaped grains; these ribbons therefore correspond to the Types III and IV ribbon morphologies of Boullier & Bouchez (1978). Ribbon-forming grains are frequently bounded by discontinuous, foliation-parallel trails of biotite grains and bulge through the gaps in these trails.

Quartz *c*-axis orientations measured on a universal stage in PSD 43W and PSSZ 95b are clustered around the mineral fibre lineations (Figs. 2a & b). In sample PSSZ 60a, *c*-axes are concentrated in discrete point maxima not distributed symmetrically about either the foliation or mineral fibre lineation (Fig. 2c). PSD 45 has a more dispersed but symmetric *c*-axis distribution about

the foliation with gaps in *c*-axis density near the mineral fibre lineation (Fig. 2d).

Boudinaged rutile grains are present as inclusions in quartz in PSSZ 60a. Using the strain reversal technique of Ferguson (1981) we estimated the orientation and magnitude of the finite strain in a thin section cut perpendicular to the foliation and parallel to the mineral fibre lineation (Fig. 3). Data were divided into quadrants (Q1–Q4), with the fourth quadrant centered perpendicular to the trace of the sample foliation. This allowed us to determine if the data were symmetrically dispersed around the foliation and, with the assumption that rutile needles had an initially random distribution and were passively reoriented during deformation, to estimate R_f, the axial ratio of the finite strain ellipse (De Paor 1981). The maximum stretch axis of the finite strain ellipse is offset by ~5° from the foliation (Fig. 3) and is consistent with an R_f value between 2.4 and 3.

Feldspar

Perthitic and antiperthitic megacrysts of feldspar are present in PSD 45 and PSD 43W in a groundmass of lamellar microperthite and plagioclase. The megacrysts are elongate in the plane of the foliation and locally ribbon-forming.

Exsolution in perthite grains produces 25–100 μm thick plagioclase blebs hosted by lamellar microperthite with exsolution lamellae about 1 μm thick. Exsolution in antiperthite grains produces coarse K-feldspar blebs. Electron microprobe traverses across individual antiperthite host grains showed no evidence of compositional zoning. Representative alkali and plagioclase feldspar compositions are in Table 2. Perthite and antiperthite megacrysts exhibit extreme intracrystalline bending (White & Mawer 1986, 1988), deformation bands and subgrains (Fig. 4a). High angle feldspar–feldspar grain boundaries are commonly sutured and associated with the nucleation of recrystallized grains (Fig. 4b). Core and mantle textures (White 1976) are also locally present (Fig. 4c). Recrystallized lamellar microperthite grains are 250–500 μm in size. Recrystallized plagioclase grains are generally 40–50 μm, but may reach 450–900 μm in the absence of recrystallized microperthite.

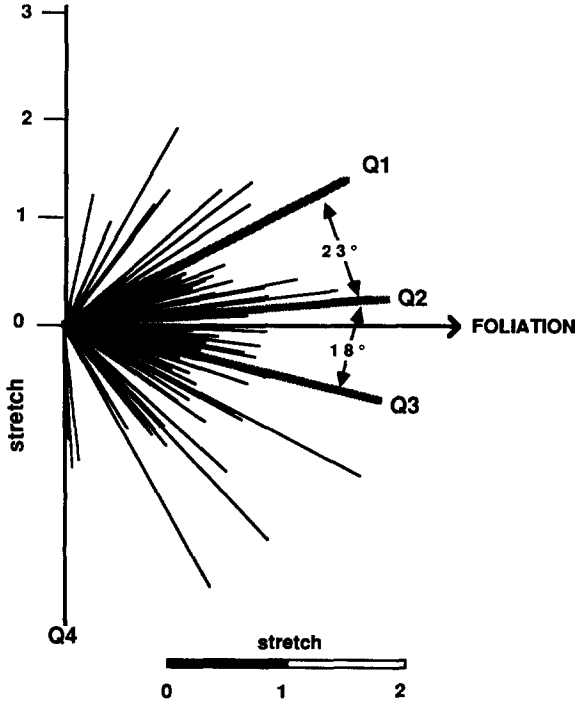

Fig. 3. Rose diagram showing the orientation and calculated stretch of boudinaged rutile inclusions in quartz in PSSZ 60a. Measurements taken from thin section cut perpendicular to foliation and parallel to mineral fiber lineation. Q1, Q2, Q3 and Q4 are quadrants separating the data into quarters following the method of De Paor (1981).

Table 2. Representative electron microprobe analyses of feldspar. 1, antiperthite host, PSD 43W; 2, recrystallized plagioclase, PSD 43W; 3, plagioclase, PSSZ 60a; 4, K-feldspar, PSSZ 60a; 5, plagioclase, PSSZ 95b

	1	2	3	4	5
NaO	8.07	7.96	7.93	0.56	7.60
MgO	0.02	0.01	0	0	0
Al_2O_3	24.40	24.39	24.49	18.49	25.25
SiO_2	61.16	61.44	60.85	64.15	60.51
K_2O	0.45	0.45	0.19	15.75	0.28
CaO	5.93	6.03	6.05	0.02	6.74
TiO	0.04	0.01	0	0.01	0
MnO	0	0.01	0	0.10	0
FeO_T^*	0.09	0.10	0.01	0.02	0.12
Total	100.15	100.4	99.52	99.11	100.49
	Cations for 8 oxygens				
Na	0.695	0.684	0.686	0.051	0.653
Mg	0.001	0	0	0	0
Al	1.278	1.273	1.288	1.015	1.319
Si	2.717	2.722	2.715	2.988	2.681
K	0.026	0.025	0.011	0.936	0.016
Ca	0.282	0.286	0.289	0.001	0.320
Ti	0.001	0	0	0	0
Mn	0	0	0	0.004	0
Fe	0.003	0.004	0.001	0.001	0.004
(Ca + Na + K) Cation sum	1.003	0.995	0.986	0.988	0.989

*All Fe reported as Fe^{2+}.

Myrmekitic intergrowths of plagioclase plus quartz are present in PSD 45 and PSD 43W. They form about 1% by volume of these samples and are developed on perthite–perthite grain boundaries both parallel and perpendicular to the foliation.

In PSSZ 60a and PSSZ 95b, plagioclase is present as lenticular, mono- and polycrystalline domains isolated in quartz. These plagioclase grains are free from optically-detectable intracrystalline strain. Domain lengths vary from 250 to 700 μm with aspect ratios of about 2:1. K-feldspar is present in PSSZ 60a as monocrystalline domains isolated in quartz and at the tips of mixed lenticular domains of plagioclase and K-feldspar. An examination of individual feldspar grains with the electron microprobe found no compositional zoning.

Grain shape analysis: domain morphology

Quartz–feldspar (Q–F) phase boundaries are gently curved and locally show cusps that point from feldspar-rich domains into quartz-rich domains (Fig. 5). Phase

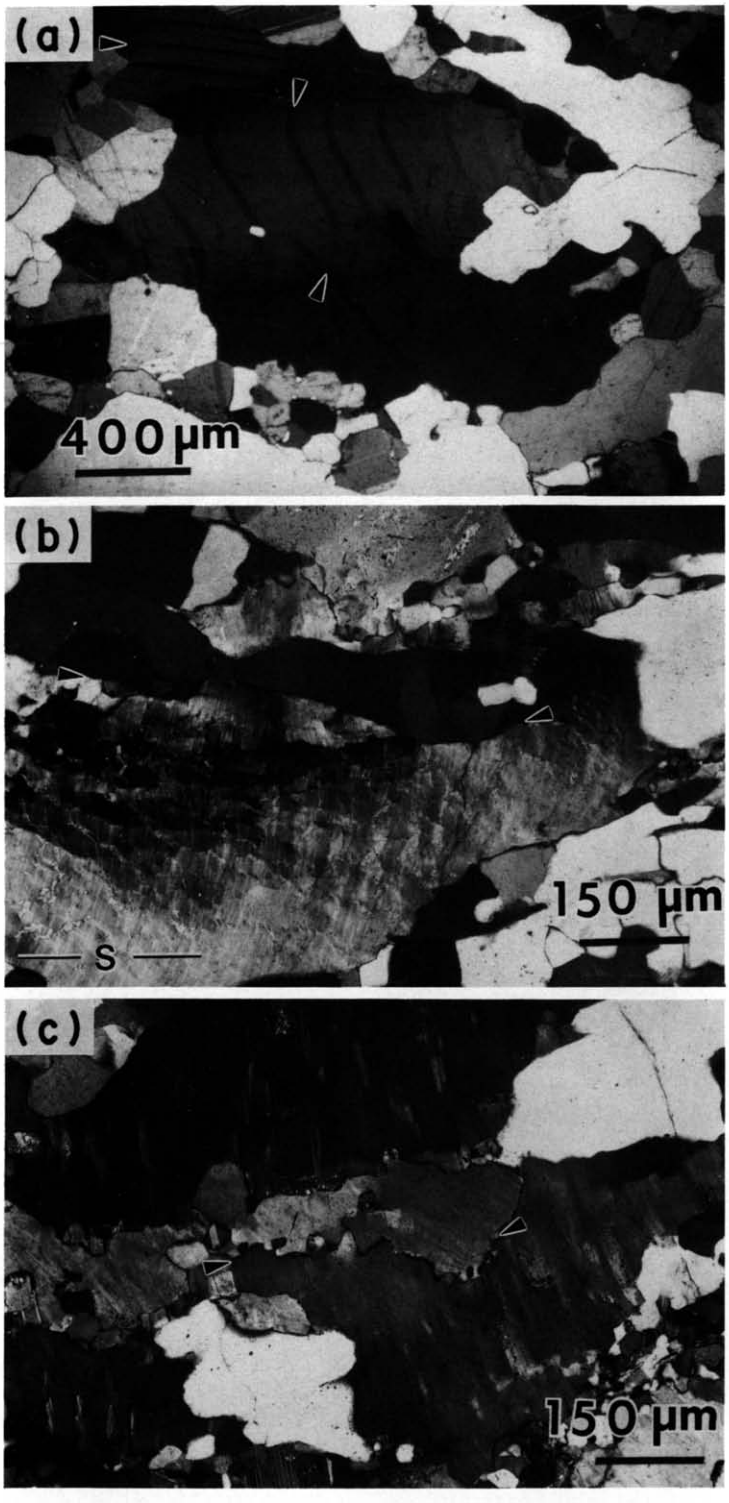

Fig. 4. Photomicrographs of (a) antiperthite megacryst with deformation twins and kinked growth twins in PSD 43W; (b) core and mantle textures in lamellar microperthite in PSD 45; arrows indicate foliation-parallel quartz–feldspar grain boundary. S = trace of foliation; and (c) sutured grain boundary between microperthite grains in PSD 45 indicated by arrows. Thin sections cut perpendicular to the foliation and parallel to the mineral fiber lineation (a & c), and perpendicular to both foliation and mineral fiber lineation (b). Nicols crossed in each case.

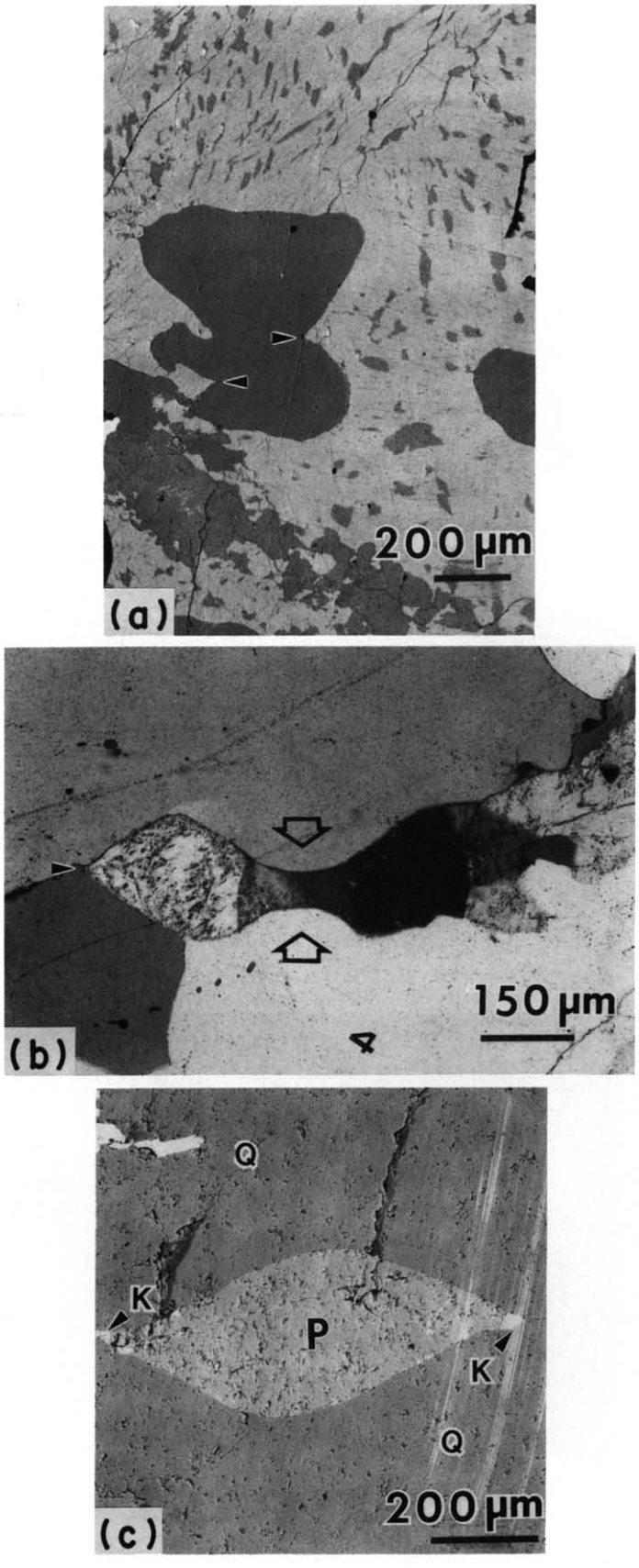

Fig. 5. Photomicrographs showing different Q–F phase boundary morphologies. (a) Backscattered scanning electron microscope (SEM) picture of isolated grain boundary cusps between quartz (Q) and perthitic alkali feldspar (F) in PSD 45. (b) Optical photomicrograph of plagioclase feldspar promontory (P) in quartz (Q) in PSD 43W. Single arrow points to the cuspate termination of promontory, which is also the site of Q–F–Q three-grain contact; double arrows indicate a pinch-and-swell structure. (c) Backscattered SEM picture of isolated lenticular plagioclase domain (P) in quartz (Q) with K-feldspar (K) present at the cusps in PSSZ 60a. Plagioclase composition in Table 2. Thin sections cut perpendicular to foliation and parallel to mineral fiber lineation (a & c), and perpendicular to both foliation and mineral fiber lineation (b). Foliation horizontal in all cases.

boundary cusps are present in thin sections cut both perpendicular and parallel to the foliation (Fig. 6). In sections cut perpendicular to the foliation they point along the plane of the foliation; in sections cut in the plane of the foliation they consistently point in the direction of the mineral fibre lineation. The morphology of phase boundaries between quartz (Q)- and feldspar (F)-rich domains is independent of the composition and structural state of feldspar adjacent to the boundary.

We have identified three morphological types of Q–F phase boundary cusp: (1) single cusps developed on an otherwise gently curved Q–F phase boundary (Fig. 5a); (2) cusps developed at the terminations of promontories of feldspar which point into quartz-rich domains (Fig. 5b); and (3) cusps associated with lenticular domains of feldspar, isolated in quartz in the plane of section (Fig. 5c). Type 2 promontories commonly have a pinch-and-swell morphology (Fig. 5b).

In PSSZ 60a, Type 3 feldspar domains have a monoclinic symmetry with their two-fold rotation axis of symmetry at a high angle to the mineral fibre lineation in the plane of the foliation (Fig. 5c). In other samples, Type 3 feldspar domains have an orthorhombic symmetry with a two-fold rotation axis of symmetry at a high angle to the mineral fibre lineation in the plane of the foliation.

Grain shape analysis: Q–F phase boundary microstructures at three-grain contacts

Cusps are commonly, but not always, the sites of three- or four-grain contacts between quartz and feldspar. To describe the geometry of three-grain contacts we use a local, right-handed orthogonal reference frame whose orientation is determined by an interfacial unit vector (**i**), which is common to all the grain boundaries at the contact, and by a unit vector (**a**), which lies in the plane of one of the grain boundaries (Hoffman & Cahn 1972) (Fig. 7a). The true interfacial angles (ϕ) at three grain contacts are observed only in the plane containing **a** whose normal is **i** (Fig. 7b). In general, therefore, the angles measured between grain boundaries at three-grain contacts in thin section are apparent rather than true interfacial angles at these contacts. True interfacial angles are estimated as the median of 45 or more measurements of apparent interfacial angles following Riegger & van Vlack (1960). This estimate has in an uncertainty of about ±10% (Riegger & van Vlack 1960). True interfacial angles at quartz–quartz–quartz (Q–Q–Q) three-grain contacts were measured in sections cut parallel to sample lineation and perpendicular to foliation. They are approximately 120° in all four samples (Table 3a). Apparent intefacial angles in feldspar at cusp-associated quartz–feldspar–quartz (Q–F–Q) three-grain contacts were measured in sections cut both parallel and perpendicular to the sample lineation, and perpendicular to foliation. The median values of datasets from these two different orientations are not significantly different within individual samples but are quite variable among the samples: they range from 45° in PSD 45 to 71° in PSSZ 95b (Table 3). Graphs of normalized cumulative frequency vs apparent interfacial angle are presented for both Q–Q–Q and Q–F–Q data sets; they show a smooth, near symmetric distribution of values

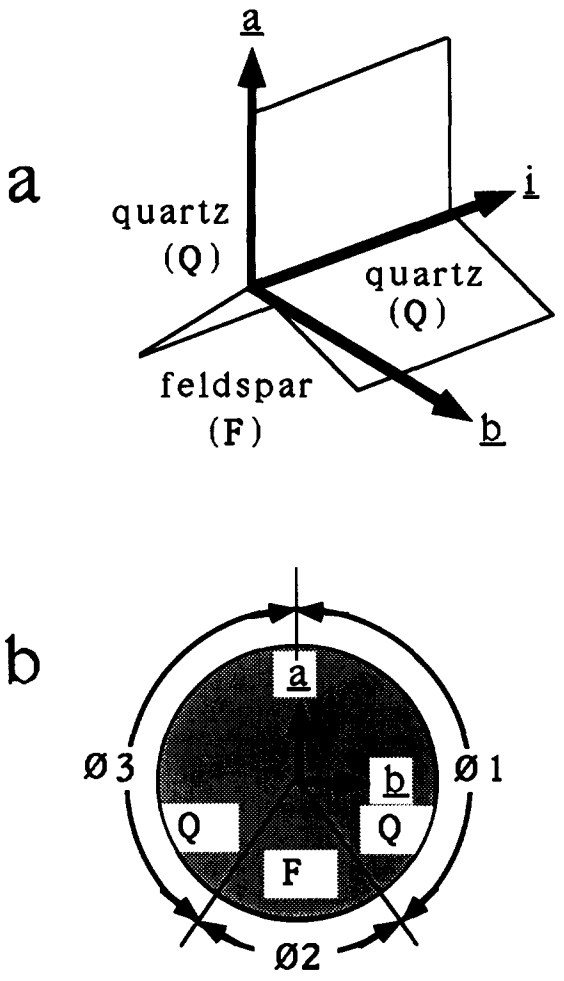

Fig. 7. Orthogonal reference frame for three grain contacts (after Hoffman & Cahn 1972). (a) Perspective view. **i**, interfacial unit vector; **a**, grain boundary unit vector; **b**, unit vector normal to **i** and **a**. (b) Plane perpendicular to **i** containing the true interfacial angles (ϕ).

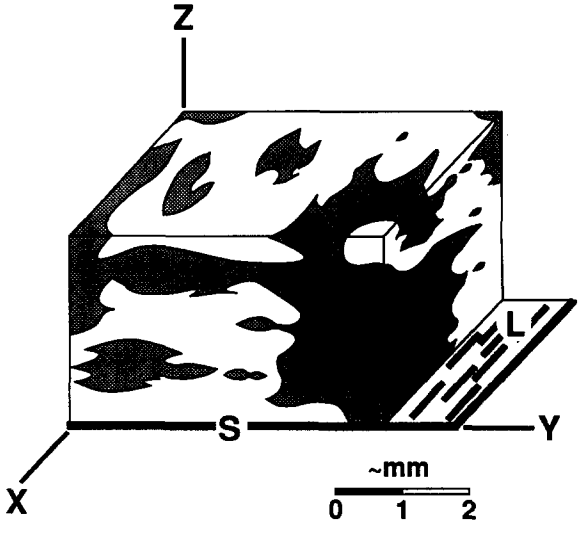

Fig. 6. Block diagram showing orientation of quartz–feldspar grain boundary cusps with respect to foliation (S) and mineral fiber lineation (L). X, Y, Z are principal stretches of finite strain ellipsoid inferred for the samples, where $X > Y > Z$.

about the median in all Q–Q–Q cases (Fig. 8a) whereas the Q–F–Q measurements show smooth distributions in PSD 43W and PSD 45 only (Fig. 8b).

DISCUSSION

Deformation and recrystallization mechanisms in Q- and F-domains

The clustering of quartz *c*-axes around the mineral fibre lineations in PSD 43W and PSSZ 95b (Figs. 2a & b) is consistent with dislocation motion on the prism ⟨*c*⟩ glide system in quartz (Lister 1981, Lister & Dornsiepen 1982) and strongly suggests that quartz accommodated some intracrystalline plastic strain by dislocation creep at deformation temperatures in excess of 500–650°C (O'Hara & Gromet 1985, Blumenfeld *et al.* 1986). The dispersed but symmetric quartz *c*-axis pattern in PSD 45 (Fig. 2d) is not consistent with a predominance of dislocation motion on any single known glide system in quartz (Blumenfeld *et al.* 1986, Schmid & Casey 1986) but is similar to the pattern predicted by Taylor–Bishop–Hill simulations using a combination of basal ⟨*a*⟩ and prism ⟨*c*⟩ glide systems (Lister 1981, fig. 2). The point maxima *c*-axis distribution in PSSZ 60a (Fig. 2c) is not consistent with progressive dislocation creep using either basal ⟨*a*⟩, prism ⟨*c*⟩, or a combination of these systems. These observations differ from previous studies of high temperature deformation in quartz-bearing rocks that found a relationship between the intensity of *c*-axis preferred orientation and quartz content (Starkey & Cutforth 1978, Lisle 1985).

Extreme lattice bending, deformation bands, subgrains and deformation twins in perthitic alkali feldspar grains in PSD 43W (Fig. 4a) and PSD 45 suggest that these grains also accommodated some intracrystalline plastic strain by dislocation creep. A similar interpretation was made from optical and TEM observation of alkali feldspars sampled in an adjacent area by White & Mawer (1986, 1988). Core and mantle textures (Fig. 4b) are similar to those described in perthites by White & Mawer (1988) and are consistent with dynamic recrystallization resulting from progressive subgrain rotation

Table 3. True interfacial angles at (a) quartz–quartz–quartz (Q–Q–Q) three-grain contacts, and (b) quartz–feldspar–quartz (Q–F–Q) cusp-associated three-grain contacts

Sample	ϕ_2 (°)	*N*	Standard Deviation (°)
(a) Q–Q–Q contacts			
PSD 45	121	144	23.6
PSD 43W	118	144	20.1
PSSZ 95b	119	309	20.0
PSSZ 60a	124	171	24.1
(b) Q–F–Q contacts			
PSD 45	45	133	18.3
PSD 43W	51	94	18.5
PSSZ 95b	71	45	38.5
PSSZ 60a	61	56	37.2

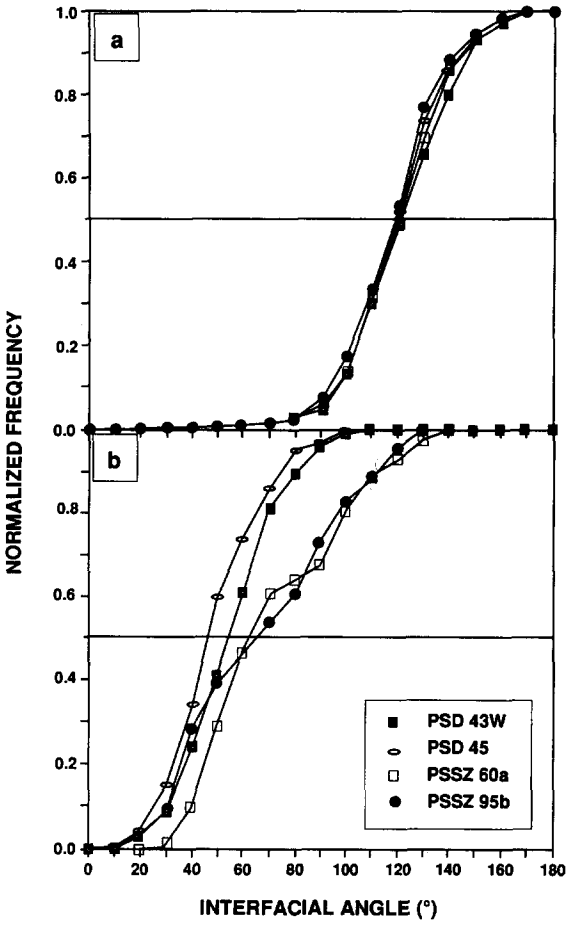

Fig. 8. Normalized frequency vs measured interfacial angle at (a) Q–Q–Q three-grain contacts and (b) Q–F–Q cusp-associated three-grain contacts.

(White 1976, Guillope & Poirier 1979). Sutured perthite–perthite grain boundaries (Fig. 4c) are consistent with grain boundary migration recrystallization (Urai *et al.* 1986).

Finite strain geometries were determined from strain analysis in PSSZ 60a (Fig. 3) and elsewhere inferred from the occurrence of foliation-parallel pinch-and-swell microstructures (Fig. 5b) that we interpret to be indicative of incipient foliation-parallel boudinage in all samples. These pinch-and-swell structures are consistent with finite shortening perpendicular to the foliation and finite extension in the foliation plane; they are observed in planes cut both parallel and perpendicular to the lineation (Fig. 6).

Several processes might account for the absence of optically-detectable intracrystalline lattice strains in plagioclase, K-feldspar and quartz in PSSZ 60a and PSSZ 95b. The most obvious, that these samples were never deformed, is untenable because strain analysis of rutile inclusions in quartz is consistent with a minimum foliation-parallel stretch in the range 2.4–3 in PSSZ 60a (Fig. 3), and the quartz *c*-axis patterns in PSD 43W and PSSZ 95b (Figs. 2a & b) are consistent with dislocation creep.

It might be argued that quartz formed an interconnected, stress-supporting matrix (Jordan 1987) in which isolated F-domains remained rigid. However, the pinch-

and-swell morphologies suggest that F-domains underwent considerable plastic strain during deformation. The deformation mechanism(s) active in F-domains must therefore have generated lattice strains that were extensively recovered during and after deformation. Alternatively, optically-detectable lattice strains were not generated in the first place. The morphology of Q–F phase boundaries and internal microstructures of F-domains allows us to distinguish between these two alternatives.

Timing of Q–F phase boundary motion with respect to deformation

The morphology of Q–F–Q three-grain contacts at some Q–F phase boundary cusps (Fig. 5b) as well as the grain shape fabrics in Q-domains (Table 3a, Fig. 8a) resemble the cuspate morphology phase and grain boundaries at three- and four-grain contacts formed during annealing of polyphase aggregates under experimental (Kingery *et al.* 1976, Jurewicz & Watson 1986, Hay & Evans 1988) and natural (Kretz 1966, Spry 1969, Vernon 1970) hydrostatic conditions. Under these conditions phase and grain boundary cusps develop at three- and four-grain contacts in all orientations (Kingery *et al.* 1976) and migrate through an aggregate as a result of diffusive mass transfer to and from the contact sites (Hunter 1987). Ultimately, when the driving forces for grain boundary motion are balanced about interfacial vectors (i) throughout the material, they achieve a steady configuration termed textural equilibrium (Kingery *et al.* 1976). At equilibrium there exists a simple relationship between the true interfacial angles (ϕ) and the driving forces for grain boundary motion (α) at three grain contacts. This relationship is given by

$$\alpha_1^2 = \alpha_2^2 + \alpha_3^2 - 2\alpha_2\alpha_3 \cos[\pi - \phi_1], \quad (1)$$

where the subscripts refer to the three grain boundaries that intersect at the contact and ϕ_1 is the true interfacial angle between grain boundaries 2 and 3.

In two-phase materials equation (1) reduces to the well-known wetting angle relationship (Kingery *et al.* 1976, p. 213)

$$\alpha_1/2\alpha_2 = \cos[\phi_1/2], \quad (2)$$

which has been used to estimate the driving forces for phase boundary motion in statically annealed mineral–mineral (Hunter 1987), mineral–fluid (Hay & Evans 1989) and mineral–melt systems (Cooper & Kohlstedt 1982, Jurewicz & Watson 1985). These studies indicate that, to a first approximation, the driving forces for phase boundary motion during static annealing depend on the phases present at three grain contacts rather than the crystallographic orientation of phases adjacent to the boundary (but see Hoffman & Cahn 1972 and Cooper & Kohlstedt 1982 for discussion of crystallographic orientation dependence of α).

In addition to the similarities between cuspate Q–F phase boundaries in our samples and texturally-equilibrated phase boundaries from other natural settings, there are some significant differences. For example, grain boundary pinning microstructures between quartz and feldspar, and the absence of Q–F–Q three-grain contacts at some Q–F phase boundary cusps suggest that textural equilibration was not attained throughout our samples. In addition, the frequency distribution of apparent interfacial angles at cusp-associated Q–F–Q contacts in PSSZ 60a and PSSZ 95b (Fig. 8b) and the intersample variation in true interfacial angles in feldspar (Table 3b) cannot be easily reconciled with textural equilibration (see Riegger & van Vlack 1960).

The preserved microstructures may have resulted from extensive post-deformational annealing that was arrested before equilibrium was attained. Quartz annealing rates are much higher than those for feldspar under the same pressure–temperature conditions, so this hypothesis is attractive as an explanation of the intersample variation in feldspar interfacial angles (Table 3b) as well as for textural equilibrium in Q-domain interiors. Bulging of Q–Q grain boundaries around F-domains and some isolated biotite grains is consistent with grain boundary pinning (Jessel 1987), which could be either syn- or post-tectonic. However, the modal volume of biotite is always low ($\leq$3%) in these samples and there are insufficient grains to pin all the phase boundaries. The morphologies of Q–F phase boundaries are thus independent of biotite distribution and yet they show a consistent relationship to the foliation and inferred strain geometry. Post-tectonic annealing should have produced phase boundary cusps in all orientations (Kingery *et al.* 1976) irrespective of the attainment of textural equilibrium. We therefore suggest that Q–F microstructures formed during deformation and were not significantly modified after deformation. The similarity of these phase boundary microstructures to those in statically annealed rocks is consistent with a process of syn-tectonic Q–F phase boundary motion similar to, but distinct from, annealing recrystallization.

DYNAMIC RECRYSTALLIZATION MODEL

The term 'dynamic recrystallization', which according to Vernon (1981, p. 605) refers to the "development and/or migration of a high angle grain boundary" through a crystalline aggregate during deformation, is not strictly applicable when the boundary separates different minerals. In these instances, however, there seems to be no universally agreed terminology. On one hand, Urai *et al.* (1986, p. 162) state that when motion occurs at "boundaries [that] separate different phases, the process [of boundary migration] is called neocrystallization or a phase transition". On the other hand, Chen (1983, p. 228) has termed phase boundary motion in polycrystalline ceramics and other materials "migration-assisted diffusional creep". We choose to retain the term 'dynamic recrystallization' here because it does not imply that phase boundary motion involved any unwar-

ranted change in bulk composition and also because it avoids an *a priori* assumption that diffusional creep was the predominant deformation mechanism in our samples.

Dynamic recrystallization of Q–F phase boundaries can be visualized using two hypothetical Q–F–Q grain boundary cusps: one initially pointing at a high angle to the foliation (Fig. 9a), the other pointing along the plane of the foliation (Fig. 9b) near parallel with the inferred *XY*-principal plane of the finite strain ellipsoid (where $X > Y > Z$). We describe phase boundary motion in a reference frame fixed to the foliation and lineation direction (Fig. 9). There are two components associated with grain distortion: a passive component determined only by the bulk velocity fields of the grains adjacent to the boundaries, and an active or migration component. The migration component results from diffusive mass transfer to, along, and away from the phase boundaries.

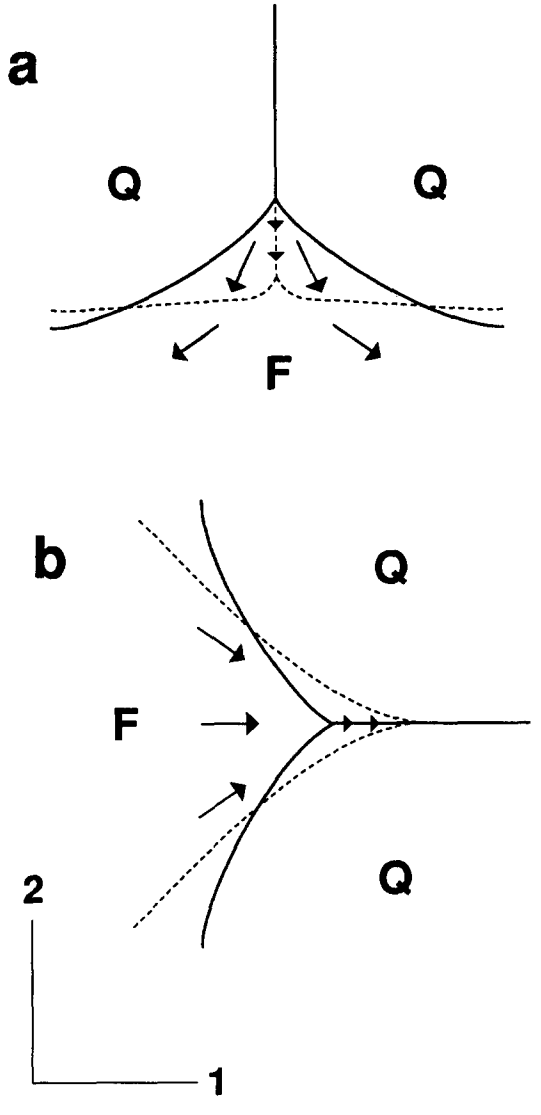

Fig. 9. Inferred motion of Q–F grain boundary cusps; (a) cusp points perpendicular to foliation (2), in direction of inferred maximum finite shortening and (b) cusp points parallel to foliation (1), in direction of inferred maximum finite extension. Large arrows indicate possible pathways for diffusive mass transfer of feldspar components. Small arrows indicate translation of three grain contact resulting from diffusional creep.

The passive component results from small elastic strains that are accumulated in all grains during deformation and large, but difficult to quantify, crystal-plastic strains accommodated by dislocation creep in quartz, plagioclase and alkali feldspar. In instances where passive phase boundary motion is predominant, and post-tectonic annealing is limited in F-domains, we expect the morphology of Q–F phase boundaries to closely reflect the grain size and shape characteristics of the F-domains adjacent to the boundary.

Because the final microstructure only contains Q–F phase boundary cusps that point along the foliation, deformation of the two hypothetical Q–F–Q cusps must result in a reduction in amplitude of the cusp at a high angle to the foliation (Fig. 9a) and an increase in amplitude of the cusp that points along the foliation (Fig. 9b). In PSD 43W and PSD 45 the preservation of delicate, dynamic recrystallization microstructures in F-domains (Figs. 4b & c) and of extreme lattice bending suggest that post-deformational annealing of feldspar was not extensive. Nevertheless Q–F phase boundaries have a gentle and consistent curvature that is independent of the grain size and shape fabrics in F-domains suggesting that active, as well as passive, phase boundary migration occurred.

The smooth curvature Q–F phase boundaries also requires more than fine-scale diffusive mass transfer over length scales of the order of individual recrystallized feldspar grains. Isolated lenticular F-domains in PSD 43W and PSD 45 are on average much larger (200 μm–2 mm long) than the near equant microperthite (250–500 μm) and plagioclase (40–50 μm) grains formed by grain boundary migration recrystallization in F-domain interiors. Hence, isolated F-domains cannot represent single dynamically recrystallized feldspar grains that were swept out into the quartz-rich matrix during deformation and subsequently modified in shape by fine-scale phase boundary migration. Instead the size and lenticular shape of these domains suggest that phase boundary migration and diffusive mass transfer were active over length scales of the order of a domain size (~200 μm–2 mm) or greater.

We propose that dynamic recrystallization of Q–F phase boundaries is indicative of a type of diffusional creep which accommodated foliation-parallel extension and foliation-perpendicular shortening of our samples. The proposed mechanism is distinct from diffusion-accommodated grain boundary sliding in quartzofeldspathic rocks (e.g. Behrmann & Mainprice 1987), which is considered unlikely in Parry Sound rocks because of the coarseness and shape of F-domains. We suggest that diffusional creep involved feldspar dissolution at foliation-parallel phase boundaries coupled with feldspar precipitation at Q–F phase boundary cusps and diffusive mass transfer between the dissolution and precipitation sites (Fig. 10). The quantitative relationship between deviatoric stress magnitude, diffusion and reaction rates are unknown, but qualitatively the strain geometries in our samples are inappropriate for compressive stresses oriented in the foliation plane.

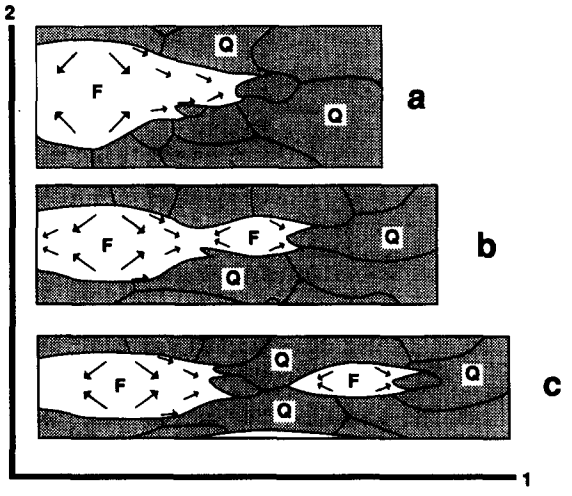

Fig. 10. Conceptual model for the formation of cuspate grain boundary microstructures between quartz- (Q) and feldspar- (F) rich domains. 2, maximum finite shortening direction; 1, maximum finite extension direction. Arrows indicate possible diffusion pathways for feldspar components through interior of feldspar-rich domains (see text for discussion of other possible pathways).

Theoretical constitutive laws for grain boundary and intracrystalline diffusional creep in metals and ceramics (Poirier 1985, pp. 194–200) suggest that if all other parameters remain constant, a monophase aggregate deforming by solid-state diffusional creep alone will favor volume diffusion over grain boundary diffusion at coarser grain sizes. Unfortunately the magnitudes of the effective grain-boundary and volume self diffusion coefficients for Si, Al, K, Na, Ca and O and their activation energies in quartz and feldspar remain poorly known (see review in Joesten 1991). Hence the relative roles of grain boundary vs volume diffusion are difficult to evaluate. In practice, diffusive mass transfer by either an intracrystalline (as illustrated schematically in Figs. 9 and 10) or gain boundary pathway is consistent with the observed textures. The textures are also consistent with a combination of intracrystalline and grain boundary diffusive mass transfer.

It is interesting to note that foliation-parallel Q–F phase boundaries have a much larger surface area than the portions of these boundaries that are cuspate and at a high angle to the foliation. A steady, volume-conserving deformation can be achieved by the proposed deformation mechanism only if the rate of feldspar precipitation per unit area of Q–F phase boundary (i.e. the specific precipitation rate, A_1) exceeds the specific rate of feldspar dissolution (A_2). Moreover, as F-domains extend in the foliation plane during progressive deformation, the ratio A_1/A_2 has to increase in order to maintain rock volume. Studies of grain boundary diffusional creep suggest that strain rates are strongly dependent on whether creep is controlled by diffusive mass transfer (Coble 1963) or the rate of vacancy production and destruction at dissolution and precipitation sites (Frost & Ashby 1982, Raj 1982). When the latter process prevails (during so-called 'interface-controlled grain boundary diffusional creep') changes in phase and grain boundary surface area during deformation are expected to result in strongly non-linear creep behavior (Lehner 1990).

We summarize textural development in our samples in Fig. 10. Stages 1 and 2 (Figs. 10a & b) occur during deformation and are cyclical. Stage 1 involves an initial extension in the plane of the foliation accommodated by dislocation creep in Q- and F-domains as well as by dissolution at foliation-parallel Q–F phase boundaries. These reactions are coupled with diffusive mass transfer to and from phase boundary reaction sites and together accommodate foliation-parallel extension of F-domains leading to the development of feldspar promontories (Fig. 10a). Stage 2 involves the development of pinch-and-swell textures at feldspar promontories and the eventual boudinage of these promontories to form isolated, lenticular, mono- and polycrystalline F-domains in a quartz-rich matrix (Figs. 10b & c).

CONCLUSIONS

We have documented the microstructural development in four mylonitic quartzofeldspathic gneisses deformed under upper amphibolite facies at temperatures in excess of 650–750°C. The morphology of Q–F grain boundaries in these rocks suggests that these boundaries were mobile during, but not after, deformation and that their motion was accommodated, in part, by feldspar dissolution at foliation-parallel Q–F grain boundaries, diffusive mass transfer over length-scales of ~200 μm–2 mm, and feldspar precipitation at Q–F grain boundary cusps that point along the foliation. These cuspate phase boundary microstructures are therefore indicative of a type of solid-state diffusional creep in quartzofeldspathic rocks deformed at elevated temperatures. The development of these textures in both feldspar-rich and feldspar-poor samples suggests that the occurrence of diffusional creep is unaffected by the feldspar content of these rocks. The diffusion pathways between dissolution and precipitation sites are poorly constrained; they probably included, but were not limited to, interior of F-domains and Q–F phase boundaries. Additional strains were accommodated in PSD 43W, PSD 45 and PSSZ 95b, by dislocation creep in quartz, and in PSD 43W and PSD 45 by dislocation creep in feldspar.

This study has implications for textural development and the controls on ductility in quartzofeldspathic rocks during deformation in the mid to lower continental crust. It provides evidence that the field of diffusional creep, previously recognized in high temperature deformation experiments with fine grained (~2–10 μm), and partially-molten quartzofeldspathic and feldspathic aggregates (Ji & Mainprice 1986, Dell'Angelo & Tullis 1988), extends to include coarse-grained quartzofeldspathic rocks deformed under natural, melt-free conditions at temperatures in excess of 650–750°C. Further microstructural studies of quartzofeldspathic rocks deformed under these conditions should establish what role, if any, transitions between diffusional and dislo-

cation creep regimes play in strain localization in the continental crust during orogenesis.

Acknowledgements—Crystallographic preferred orientations were determined optically with the FUTRON™ automated universal stage at Johns Hopkins University using software developed by D. De Paor. Mineral analyses and backscattered SEM images were obtained using the JEOL JXA-8600 electron microprobe at Johns Hopkins University with natural standards and ZAF reduction programs with the assistance of Albert Leger and Greg Symmes. This work was supported by NSF grant EAR 89-16354 (awarded to C. Simpson).

The authors wish to thank David Sanderson and two anonymous reviewers for their constructive comments.

REFERENCES

Anovitz, L. & Essene, E. 1990. Thermobarometry and pressure–temperature paths in the Grenville Province of Ontario. *J. Petrol.* **31**, 197–241.

Beach, A. 1976. The interactions of fluid transport, deformation, geochemistry and heat flow in early Proterozoic shear zones, Lewisian complex. *Phil. Trans. R. Soc. Lond.* **A280**, 569–604.

Behrmann, J. H. & Mainprice, D. 1987. Deformation mechanisms in a high temperature quartz–feldspar mylonite: evidence for superplastic flow in the lower crust. *Tectonophysics* **140**, 297–305.

Blumenfeld, P., Mainprice, D. & Bouchez, J.-L. 1986. C-slip in quartz from subsolidus deformed granite. *Tectonophysics* **127**, 97–115.

Boullier, A. M. & Bouchez, J.-L. 1978. Le quartz en rubans dans les mylonites. *Bull. Soc. géol. Fr.* **7**, 253–262.

Burg, J.-P., Wilson, C. J. L. & Mitchell, J. C. 1986. Dynamic recrystallization and fabric development during simple shear deformation of ice. *J. Struct. Geol.* **8**, 857–870.

Chen, I.-W. 1983. Effects of boundary mobility and phase equilibration on kinetic processes of multicomponent polyphase ceramics. In: *The Character of Grain Boundaries* (edited by Yan, M. F. & Heuer, A. H.). *Adv. Ceramics* **6**, 224–235.

Coble, R. L. 1963. A model for boundary-diffusion controlled creep in polycrystalline materials. *J. appl. Phys.* **34**, 1679–1682.

Cooper, R. F. & Kohlstedt, D. L. 1982. Interfacial energies of olivine–basalt partial melts. *J. geophys. Res.* **91**, 9315–9323.

Culshaw, N. G., Check, G., Corrigan, D., Drage, J., Gower, R., Haggart, M. J., Wallace, P. & Wodicka, N. 1988. Georgian Bay geological synthesis: Dillon to Twelve Mile Bay, Grenville Province of Ontario. *Geol. Surv. Pap. Can.* **89-1C**, 157–163.

Davidson, A. 1984. Identification of ductile shear zones in the southwestern Grenville Province of the Canadian shield. In: *Precambrian Tectonics Illustrated* (edited by Kroner, A. & Greiling, R.). E. Schweizerbart'sche, Stuttgart, 263–279.

Dell'Angelo, L. N. & Tullis, J. A. 1988. Experimental deformation of partially melted granitic aggregates. *J. metamorph. Geol.* **6**, 495–515.

De Paor, D. G. 1981. Strain analysis using deformed line distributions. *Tectonophysics* **73**, T9–T14.

Dipple, G. M., Wintsch, R. P. & Andrews, S. 1990. Identification of the scales of differential element mobility in a ductile fault zone. *J. metamorph. Geol.* **8**, 645–661.

Drury, M. R., Humphreys, F. J. & White, S. H. 9185. Large strain deformation studies using polycrystalline magnesium as a rock analogue. Part II: dynamic recrystallization mechanisms at high temperature. *Phys. Earth & Planet. Interiors* **40**, 208–222.

Ferguson, C. C. 1981. A strain reversal method for estimating extension from fragmented inclusions. *Tectonophysics* **79**, T43–T52.

Ferry, J. M. & Spear, F. S. 1978. Experimental calibration of the partitioning of Fe and Mg between biotite and garnet. *Contr. Miner. Petrol.* **66**, 1100–1106.

Frost, H. J. & Ashby, M. F. 1982. *Deformation-mechanism Maps*. Pergamon Press, Oxford.

Gandais, M. & Willaime, C. 1984. Mechanical properties of feldspars. In: *Feldspars and Feldsparthoids* (edited by Brown, W. L.). D. Reidel, Dordrecht, 207–246.

Guillope, M. & Poirier, J. P. 1979. Dynamic recrystallization during creep of single crystalline halite: an experimental study. *J. geophys. Res.* **84**, 5557–5567.

Hay, R. S. & Evans, B. 1988. Intergranular distribution of pore fluid and the nature of high angle grain boundaries in limestone and marble. *J. geophys. Res.* **93**, 8959–8974.

Hodges, K. V. & Spear, F. S. 1982. Geothermometry, geobarometry and the Al_2SiO_5 triple point at Mt. Moosilauke, New Hampshire. *Am. Miner.* **67**, 1118–1134.

Hoffman, D. W. & Cahn, J. W. 1972. A vector thermodynamics for anisotropic surfaces. Part I: fundamentals and applications to plane surface junctions. *Surface Sci.* **31**, 368–388.

Hunter, R. H. 1987. Textural equilibrium in layered rocks. In: *Origins of Igneous Layering* (edited by Parsons, I.). *N.A.T.O. Adv. Sci. Inst.* **C196**, 473–503.

Jessel, M. W. 1987. Grain boundary migration microstructures in a naturally deformed quartzite. *J. Struct. Geol.* **9**, 1007–1014.

Ji, S. & Mainprice, D. 1986. Transition from power law to Newtonian creep in experimentally deformed dry albite. *Trans. Am. Geophys. Union* **67**, 1235.

Ji, S. & Mainprice, D. 1988. Natural deformation fabrics of plagioclase: implications for slip systems and seismic anisotropy. *Tectonophysics* **147**, 145–163.

Joesten, R. 1991. Grain-boundary diffusion kinetics in silicate and oxide minerals. In: *Diffusion, Atomic Ordering, and Mass Transport; Selected Topics in Geochemistry* (edited by Ganguly, J.). *Adv. Phys. Geochem.* **8**, 345–395.

Jordan, P. G. 1987. The deformational behavior of bimineralic limestone–halite aggregates. *Tectonophysics* **135**, 185–197.

Jurewicz, S. R. & Watson, E. B. 1985. The distribution of partial melt in a granitic system: the application of liquid phase sintering theory. *Geochim. cosmochim. Acta* **49**, 1109–1121.

Kingery, W. D., Bowen, H. K. & Uhlmann, D. R. 1976. *Introduction to Ceramics*. Wiley, New York.

Kretz, R. 1966. Interpretation of the shape of mineral grains in metamorphic rocks. *J. Petrol.* **7**, 68–94.

Lehner, F. K. 1990. Thermodynamics of rock deformation by pressure solution. In: *Deformation Processes in Minerals, Ceramics and Rocks* (edited by Barber, D. J. & Meredith, P. G.). Unwin Hyman, London, 296–333.

Lisle, R. J. 1985. The effect of composition and strain on quartz-fabric intensity in pebbles from a deformed conglomerate. *Geol. Rdsch.* **74**, 657–663.

Lister, G. S. 1981. The effect of the basal-prism mechanism switch on fabric develoment during plastic deformation of quartzite. *J. Struct. Geol.* **3**, 67–75.

Lister, G. S. & Dornsiepen, U. L. 1982. Fabric transitions in the Saxony granulite terrane. *J. Struct. Geol.* **4**, 81–92.

Montardi, Y. & Mainprice, D. 1987. A transmission electron microscopic study of the natural plastic deformation of calcic plagioclases (An 68–70). *Bull. Mineral.* **110**, 1–14.

Mosher, S. 1981. Pressure solution deformation of the Purgatory Conglomerate from Rhode Island (U.S.A.): quantification of volume change, real stains and sedimentary shape factors. *J. Geol.* **89**, 37–55.

O'Hara, K. & Gromet, L. P. 1985. Two distinct Precambrian (Avalonian) terranes in southeastern New England and their late Paleozoic juxtaposition. *Am. J. Sci.* **285**, 673–709.

Olsen, T. S. & Kohlstedt, D. L. 1984. Analysis of dislocations in some naturally deformed plagioclase feldspars. *Phys. Chem. Miner.* **11**, 153–160.

Poirier, J. P. 1985. *Creep of Crystals: High-temperature Deformation Processes in Metals, Ceramics and Minerals*. Cambridge University Press, Cambridge.

Raj, R. 1982. Creep in polycrystalline aggregates by matter transport through a liquid phase. *J. geophys. Res.* **87**, 4731–4739.

Riegger, O. K. & van Vlack, L. H. 1960. Dihedral angle measurements. *Trans. metall. Soc. A.I.M.E.* **218**, 933–935.

Schmid, S. M. & Casey, M. 1986. Complete fabric analysis of some commonly observed quartz c-axis patterns. In: *Mineral and Rock Deformation Studies—The Paterson Volume* (edited by Heard, H. C. & Hobbs, B. E.). *Am. Geophys. Un. Geophys. Monogr.* **36**, 263–286.

Schmid, S. M., Panozzo, R. & Bauer, S. 1987. Simple shear experiments on calcite rocks: rheology and microfabric. *J. Struct. Geol.* **9**, 747–778.

Schwerdtner, W. M. 1987. Interplay between ductile shearing in the Proterozoic crust of the Muskoka-Parry Sound region, Central Ontario. *Can. J. Earth Sci.* **24**, 1506–1523.

Spry, A. 1969. *Metamorphic Textures*. Pergamon Press, Oxford.

Starkey, J. & Cutforth, C. 1978. A demonstration of the interdependence of the degree of quartz preferred orientation and the quartz content of deformed rocks. *Can. J. Earth Sci.* **15**, 841–847.

Tullis, J. A. 1990. Experimental studies of deformation mechanisms and microstructures in quartzo-feldspathic rocks. In: *Deformation Processes in Minerals, Ceramics and Rocks* (edited by Barber, D. J. & Meredith, P. G.). Unwin Hyman, London, 190–227.

Tullis, J. A. & Yund, R. A. 1985. Dynamic recrystallization in feldspar: a mechanism for ductile shear zone formation. *Geology* **13**, 238–241.

Urai, J. L. 1983. Water-assisted dynamic recrystallization and weakening in polycrystalline bischofite. *Tectonophysics* **96**, 125–127.

Urai, J. L., Means, W. D. & Lister, G. S. 1986. Dynamic recrystallization in minerals. In: *Mineral and Rock Deformation Studies—The Paterson Volume* (edited by Heard, H. C. & Hobbs, B. E.). *Am. Geophys. Un. Geophys. Monogr.* **36**, 161–199.

van Breeman, O., Davidson, A., Loveridge, W. D. & Sullivan, R. W. 1986. U–Pb zircon geochronology of Grenville tectonites, granulites and igneous precursors, Parry Sound, Ontario. In: *The Grenville Province* (edited by Moore, J. M., Davidson, A. & Baer, A. J.). *Spec. Pap. geol. Ass. Can.* **31**, 61–74.

Vernon, R. H. 1970. Comparative grain boundary studies of some basic and ultrabasic granulites, nodules and cumulates. *Scott. J. Geol.* **6**, 337–351.

Vernon, R. H. 1981. Optical microstructures of partly recrystallized calcite in some deformed marbles. *Tectonophysics* **78**, 601–612.

Walton, M., Mills, A. & Hansen, E. 1964. Compositionally zoned granitic pebbles in three metamorphosed conglomerates. *Am. J. Sci.* **262**, 1–25.

White, J. C. & Mawer, C. K. 1986. Extreme ductility of feldspars from a mylonite, Parry Sound, Canada. *J. Struct. Geol.* **8**, 133–143.

White, J. C. & Mawer, C. K. 1988. Dynamic recrystallization and associated exsolution in perthites: evidence of deep crustal thrusting. *J. geophys. Res.* **93**, 325–337.

White, S. H. 1976. The effects of strain on the microstructures, fabrics and deformation mechanisms in quartzites. *Phil. Trans. R. Soc. Lond.* **A283**, 69–86.

Wynne-Edwards, H. R. 1972. The Grenville Province. In: *Variations in Tectonic Style in Canada* (edited by Price, R. A. & Douglas, R. J.). *Spec. Pap. geol. Ass. Can.* **11**, 263–334.

APPENDIX

Sample description

(i) PSD 45: pink, quartzofeldspathic gneiss (34 vol.% quartz, 42% perthitic alkali feldspar, 19% plagioclase, 3% biotite, accessory garnet, ilmenite, chlorite, apatite and zircon).

(ii) PSD 43W: pink, syntectonic, quartzofeldspathic pegmatite (54% quartz, 45% perthitic and antiperthitic feldspar, accessory biotite, calcite, chlorite and zircon). The sample was collected from the limb of an intrafolial fold whose axis was parallel to the fibre lineation recorded in the sample.

(iii) PSSZ 60a: quartz-rich gneiss (94% quartz, 4% plagioclase and K-feldspar, 1.5% biotite, accessory ilmenite, zircon, apatite, chlorite).

(iv) PSSZ 95b: quartz-rich gneiss (90% quartz, 7% plagioclase, 2.5% biotite, accessory garnet, ilmenite, zircon, apatite).